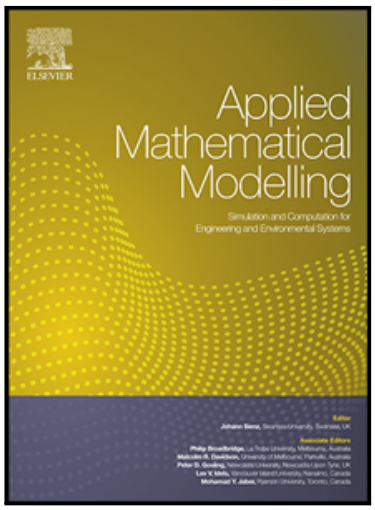

Vibration of Viscoelastic Axially Graded Beams with Simultaneous Axial and Spinning Motions under an Axial Load

A. Ebrahimi-Mamaghani , A. Forooghi , H. Sarparast ,
A. Alibeigloo , M.I. Friswell

PII: S0307-904X(20)30480-7
DOI: https://doi.org/10.1016/j.apm.2020.08.041
Reference: APM 13612

To appear in: *Applied Mathematical Modelling*

Received date: 20 January 2020
Revised date: 7 August 2020
Accepted date: 23 August 2020

Please cite this article as: A. Ebrahimi-Mamaghani , A. Forooghi , H. Sarparast , A. Alibeigloo , M.I. Friswell , Vibration of Viscoelastic Axially Graded Beams with Simultaneous Axial and Spinning Motions under an Axial Load, *Applied Mathematical Modelling* (2020), doi: https://doi.org/10.1016/j.apm.2020.08.041

Highlights

- Dynamics of viscoelastic AFG beams with axial and spinning motion is studied
- Numerical and analytical methods for determining the stability threshold are given
- Divergence and flutter analysis for the system are performed
- Influence of viscosity and axial load on the stability evolution is discussed
- Mass-addition and stiffness-hardening effects of material gradation are found

Vibration of Viscoelastic Axially Graded Beams with Simultaneous Axial and Spinning Motions under an Axial Load

A. Ebrahimi-Mamaghani[a], A. Forooghi[a], H. Sarparast[a], A. Alibeigloo[a], M.I. Friswell[b,1]

[a] *Department of Mechanical Engineering, Tarbiat Modares University, Tehran, Iran*

[b] *College of Engineering, Swansea University, Swansea, United Kingdom*

Abstract

For the first time, the structural dynamics and vibrational stability of a viscoelastic axially functionally graded (AFG) beam with both spinning and axial motions subjected to an axial load are analyzed, with the aim to enhance the performance of bi-gyroscopic systems. A detailed parametric study is also performed to emphasize the influence of various key factors such as material distribution type, viscosity coefficient, and coupled rotation and axial translation on the dynamical characteristics of the system. The material properties of the system are assumed to vary linearly or exponentially in the longitudinal direction with viscoelastic effects. Adopting the Laplace transform and a Galerkin discretization scheme, the critical axial and spin velocities of the system are obtained. An analytical approach is applied to identify the instability thresholds. Stability maps are examined, and for the first time in this paper, it is demonstrated that the stability evolution of the system can be altered by fine-tuning of axial grading or viscosity of the material. The variation of density and elastic modulus gradient parameters are found to have opposite effects on the divergence and flutter boundaries of the system. Furthermore, the results indicate that the destabilizing effect of the axial compressive load can be significantly alleviated by the simultaneous determination of density and elastic modulus gradation in the axial direction of the system.

Keywords: axially functionally graded material, viscoelastic effect, axially moving and spinning beam, divergence and flutter instability, stability map, structural dynamics

[1] Corresponding author. E-mail address: m.i.friswell@swansea.ac.uk

1. Introduction

The dynamics of axially moving structures has been the subject of numerous scientific studies over recent years [1-3]. Comprehensive reviews on the vibration and stability characteristics of axially moving systems can be found in the work of Marynowski and Kapitaniak [4], and Chen [5]. Ghayesh and Amabili [6] studied the forced dynamics and stability of translating Timoshenko beams with intra-span spring supports. They demonstrated that by increasing the axial velocity of the beam, softening behaviour could be observed in the system. Nonlinear forced vibration of axially moving Timoshenko beams with internal resonance was investigated by Ghayesh and Amabili [7]. They solved the equations of the system utilizing the direct time integration and pseudo-arclength continuation approaches. They also obtained the bifurcation diagrams, Poincare maps, and phase plane portraits for the system. Stability and post-buckling bifurcations of translating beams at high axial velocities were investigated analytically by Ghayesh and Amabili [8]. They illustrated that increasing the axial velocity leads to the disappearance of the higher-order bifurcations. The dynamics of rotating structures have been investigated by numerous researchers due to their wide applications in different engineering branches. Within this context, the influence of various key factors such as temperature gradient [9, 10], rotation axis direction [11], asymmetric geometry [12], rotating velocity fluctuation [13], size-dependent effects [14], and nonlinear absorbers [15] on the dynamical response of rotating systems have been extensively reported in the engineering literature.

Functionally graded (FG) materials are an advanced class of composite materials whose thermomechanical properties vary smoothly and continuously in a preferred direction of the structure [16-23]. Compared with homogeneous and conventional laminated materials, FG materials display unique features such as higher fracture toughness, lower stress concentration, better corrosion and thermal resistance. Ghayesh [24] surveyed the nonlinear size-dependent dynamics of viscoelastic FG beams based on couple stress theory. He investigated the effect of different parameters such as viscosity, gradient index, excitation frequency, and harmonic load amplitude on the forced response of the longitudinal and transverse displacements of the system. The nonlinear mechanical response of viscoelastic FG imperfect micro-beams was examined by Ghayesh [25]. His results disclosed that the viscosity and the geometric imperfection have considerable effects on the size-dependent forced vibration of the system. The nonlinear

vibration of AFG tapered beams subjected to harmonic excitation was modelled by Ghayesh [23]. He examined the effect of various parameters such as taper ratio and power index on the amplitude-frequency diagrams. He also showed that by adjusting the material and geometric characteristics, one could tailor the vibration of the system. As a result, utilizing FG materials in axially moving systems could lead to outstanding performance benefits. In this field, Piovan and Sampaio [26] inspected the vibrations of axially moving flexible FG beams by employing the finite element method. Their results proved that utilizing metal as the main component of the beam, compared to ceramic, leads to a lower oscillation frequency in the system. Kiani [27] surveyed the transverse and longitudinal instabilities of moving nanobeams made of FG materials. His results showed that the influence of small-scale parameters on the natural frequencies of the moving FG nanobeam depends significantly on the order of the mode and the velocity of the system. Sui et al. [28] modelled the free lateral vibration of axially moving FG beams using the Timoshenko beam theory. They evaluated the effect of diverse parameters such as the axial velocity and the power-law index on the fundamental frequency of the system. Yan et al. [29] considered the stability of moving FG beams with time-dependent axial velocity. They applied the direct multiscale method to determine the stability boundaries of the system. By increasing the axial velocity and support stiffness parameter, the instability threshold of the system decreases and increases, respectively.

The combination of FG materials and spinning structures is examined by several authors [30]. For instance, Li and Zhang [31] interpreted the dynamical response characteristics of spinning tapered AFG beams using the B-spline approach. They addressed the influence of the taper ratio, material heterogeneity, hub radius, and spin velocity on the dynamics of the system. Shafiei et al. [32] focused on the size-dependent vibrational characteristics of a non-uniform spinning FG microbeam based on the modified couple stress theory. They asserted that by considering small-size effects, the influence of shear deformation on the dynamical behaviour of the system is more significant. Ebrahimi and Mokhtari [33] assessed the free transverse vibrational behaviour of rotating FG porous Timoshenko beams using the semi-analytical differential transform method. In contrast to the slenderness ratio effect, the variation of the power-law index could considerably affect the dynamical behaviour of the system. Zarrinzadeh et al. [34] exploited the finite element method to analyze the free vibration of spinning tapered FG beams with various

boundary conditions. They explored the effect of the rotating velocity parameter, material heterogeneity, and the taper ratio on the dynamics of the system. Oh et al. [35] carried out a numerical investigation on the thermoelastic stability of thin-walled whirling FG circular beams. They demonstrated that the variation of the power index could significantly change the stability boundaries of the system. Ramesh and Rao [36] obtained the natural frequencies of pre-twisted rotating FG cantilevered beams. They investigated the coupling between the flapwise and chordwise bending modes on the dynamical response of the system for various material gradients. Oh et al. [37] performed a comprehensive study on the vibrations of turbomachinery rotating blades made of FG material and operating at high temperatures. They determined the effective material properties via the simple rule of mixtures and the Mori-Tanaka procedure. Azimi et al. [38] scrutinized the thermomechanical vibrations of rotating AFG Timoshenko nanobeams. They deduced that when the temperature is lower than the critical value, the fundamental vibrational frequency of the system decreases when the nonlocal parameter increases. Librescu et al. [39] simulated the dynamics of rotating thin-walled FG beams in a thermal environment. They concluded that the temperature gradient, as well as the alteration in material properties, play key roles in the determination of the critical buckling velocities of the system.

Axially moving and spinning beams are one of the most critical elements in the design of mechanical and aerospace structures. Due to the combination of axial and spinning motions of these practical systems, they have rich dynamics amongst all of the gyroscopic systems that are ubiquitous in engineering. Despite the importance of the mathematical modelling and simulation analysis of these structures, only a few investigations have been conducted in this field. Yuh and Young [40] investigated the dynamical modelling of an axially moving and spinning beam through experimental and simulation approaches. They revealed that at high axial velocities, the inertia force effect on the oscillation of the system is significant. Based on the Euler-Bernoulli beam theory, the vibrational response of pre-twisted moving and rotating cantilevered beams was studied by Lee [41]. He illustrated that for relatively fast whirling and axial motions, the tip displacement of the system exhibits an apparent oscillatory behaviour. Zhu and Chang [42] extended Rayleigh beam theory and analytically investigated the stability of axially moving and whirling beams. They indicated that by increasing the rotary inertia factor, the stability

boundaries of the system shrink. Yang et al. [43] studied the dynamics of axially moving and spinning beams. They obtained the natural frequencies and bifurcation points of the system for variations of axial and rotational velocities. Ghayesh et al. [44] computed the nonlinear vibration of a rotor with axial motion. They calculated the nonlinear frequencies and stability conditions of the steady-state response of the system via the multiple scales method. Sahebkar et al. [45] discussed the nonlinear vibration of an axially moving drill string in an inclined well. They explained the influence of unbalanced mass and the nonlinear force of the fluid on the nonlinear modes of the system. Unlike moving and spinning homogeneous structures, the existing literature on the vibrational analysis of axially moving and spinning composite systems is limited. Recently, Li et al. [46] determined the coupled vibrational characteristics of an axially moving and spinning thin-walled composite beam. They presented a numerical study to show the effect of geometry characteristics such as thickness- and length-to-radius ratios, as well as material characteristics such as the fiber orientation angles, on the dynamical behaviour of the system.

To the best of the authors' knowledge, the stability and vibrational analysis of viscoelastic AFG beams with both axial and rotational motions subjected to axial loads has not been discussed. Also, the effect of axial loads and utilizing viscoelastic AFG materials on the vibrational behaviour and dynamical stability of bi-gyroscopic systems has not been reported. Therefore, the main motivation of this paper is to evaluate the impact of axial loads and the application of viscoelastic AFG materials on the stability improvement of structures with simultaneous axial and rotational motion. In section 2, the dynamical equations of the system are derived using Hamilton's principle. Then, in section 3, the dynamical equations of motion of the system transformed into the Laplace domain. The Galerkin technique is utilized to extract the reduced-order model. In section 4, the stability conditions of the system are presented. In section 5, to verify the accuracy of the utilized method in the present study, the obtained results are compared with those reported in the literature. Afterward, the influence of material gradation, material distribution type, axial load, and axial and rotation motion on the dynamical characteristics and stability boundaries of the system are described and highlighted in detail. The divergence instability borders of the system are obtained numerically and analytically. Also, for the first

time, it is demonstrated that by using viscoelastic AFG material, the stability evolution of the axially moving and spinning beams can be altered.

2. Problem formulation

A schematic view of a viscoelastic AFG simply-supported beam with both axial and spinning motion is given in Figure 1. The beam moves along its axial direction with constant velocity, *u*, and spins with constant spin velocity, Ω, simultaneously. The beam is of length *L*, and an axial load, *P*, is applied at the ends of the system.

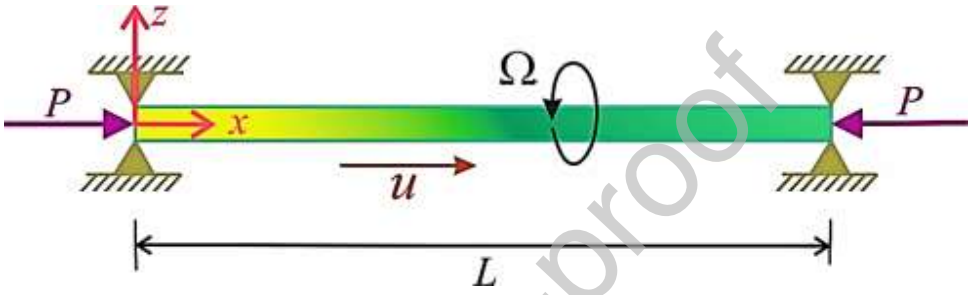

Fig. 1 Schematic view of a viscoelastic AFG beam with both axial and spinning motions under an axial load

The beam is symmetric in the longitudinal direction. The cross-sectional area, *A*, and the moment of inertia, *I*, of the system are constant in the axial direction. Also, it is assumed that the density, $\rho(x)$, and elastic modulus of the beam, $E(x)$, change linearly or exponentially in the *x*-direction as:

$$\rho(x) = \rho_0 g(x)\,, \tag{1}$$

$$E(x) = E_0 f(x)\,, \tag{2}$$

where ρ_0 and E_0 are the density and elastic modulus at the left end of the beam (x=0).

For the linear distribution:

$$g(x) = 1 + \frac{x}{L}\left(\alpha_\rho - 1\right), \tag{3}$$

$$f(x) = 1 + \frac{x}{L}(\alpha_E - 1)\,. \tag{4}$$

For the exponential distribution:

$$g(x) = e^{\frac{x\ln(\alpha_\rho)}{L}}, \tag{5}$$

$$f(x) = e^{\frac{x\ln(\alpha_E)}{L}}\,. \tag{6}$$

In Eqs. (3) - (6), α_ρ and α_{E} are the density and elastic modulus gradient parameters, respectively. They are determined as:

$$\alpha_\rho = \frac{\rho_L}{\rho_0}, \tag{7}$$

$$\alpha_E = \frac{E_L}{E_0}, \tag{8}$$

where ρ_{L} and E_{L} are the density and elastic modulus at the right end of the beam, respectively.

In practice, although the transverse motion is usually coupled with the axial motion, the axial displacement is negligible compared to the transverse displacement [8]. As a result, the transverse motion is only considered in the present study. By considering the linear strain-displacement relation, as well as the constitutive equation of the viscoelastic material based on the Kelvin-Voigt model, one obtains [47-52]:

$$\varepsilon_{\mathrm{x}} = -z\frac{\partial^2 w}{\partial x^2} - y\frac{\partial^2 v}{\partial x^2}, \tag{9}$$

$$\sigma_{\mathrm{x}} = E(x)\varepsilon_{\mathrm{x}} + \beta\frac{\mathrm{D}}{\mathrm{D}t}\varepsilon_{\mathrm{x}}, \tag{10}$$

where v and w are the transverse displacements of the beam in the y- and z-directions, respectively. Here, β, ε_{x}, and σ_{x} are the viscosity coefficient, the longitudinal strain, and the axial stress, respectively. The potential energy of the system is computed as [53]:

$$V = \frac{1}{2}\int_0^L \sigma_{\mathrm{x}}\varepsilon_{\mathrm{x}} A \mathrm{d}x\,. \tag{11}$$

By ignoring the axial displacement of the system, the kinetic energy of the system can be expressed as [43]:

$$T = \frac{1}{2}\int_0^L \rho(x)A\left(u^2 + \left(\frac{\partial v}{\partial t} + u\frac{\partial v}{\partial x} - \Omega w\right)^2 + \left(\frac{\partial w}{\partial t} + u\frac{\partial w}{\partial x} + \Omega v\right)^2\right)\mathrm{d}x\,. \tag{12}$$

Also, the work done by the axial load can be obtained as [54]:

$$W_{\mathrm{P}} = \frac{1}{2}\int_0^L P\left(\left(\frac{\partial v}{\partial x}\right)^2 + \left(\frac{\partial w}{\partial x}\right)^2\right)\mathrm{d}x\,. \tag{13}$$

To derive the dynamical equations of motion of the system, the extended Hamilton's principle is utilized:

$$\delta\int_{t_1}^{t_2}(T + W_{\mathrm{P}} - V)\,\mathrm{d}t = 0\,. \tag{14}$$

Substituting Eqs. (11) - (13) into Eq. (14), the governing dynamical equations of motion of the system are obtained as:

$$\rho(x)A(\ddot{v}+2u\dot{v}'-2\Omega\dot{w}+u^2v''-2u\Omega w'-\Omega^2v)+\rho'(x)Au(\dot{v}+uv'-\Omega w)+Pv'' + E(x)Iv''''+2E'(x)Iv'''+E''(x)Iv''+\beta I(\dot{v}''''+uv'''''')=0\,, \tag{15}$$

$$\rho(x)A(\ddot{w}+2u\dot{w}'+2\Omega\dot{v}+u^2w''+2u\Omega v'-\Omega^2w)+\rho'(x)Au(\dot{w}+uw'+\Omega v)+Pw'' + E(x)Iw''''+2E'(x)Iw'''+E''(x)Iw''+\beta I(\dot{w}''''+uw'''''')=0\,, \tag{16}$$

where the prime and dot signify the spatial and temporal derivatives, respectively.

To extract the dimensionless equations of motion, the dimensionless parameters are given as:

$$x^*=\frac{x}{L}\,,\quad v^*=\frac{v}{L}\,,\quad w^*=\frac{w}{L}\,,\quad t^*=\frac{t}{L^2}\sqrt{\frac{E_0I}{\rho_0A}}\,,\quad u^*=uL\sqrt{\frac{\rho_0A}{E_0I}},$$

$$\Omega^*=\Omega L^2\sqrt{\frac{\rho_0A}{E_0I}}\,,\quad P^*=\pm\frac{PL^2}{E_0I}\,,\quad \eta=\frac{\beta\sqrt{I}}{L^2\sqrt{\rho_0AE_0}}\,,\quad \lambda(x^*)=g'(x)L\,, \tag{17}$$

$$\gamma(x^*)=f'(x)L\,,\quad \mu(x^*)=f''(x)L^2\,.$$

It should be mentioned that in the dimensionless axial load parameter (P^*), the positive and negative signs refer to compressive and tension loads, respectively.

By substituting the dimensionless parameters of Eq. (17) into the dynamical equations of motion of the system and eliminating the asterisk notation from dimensionless parameters, the non-dimensional form of the dynamical equations of motion the system can be obtained as:

$$g(x)(\ddot{v}+2u\dot{v}'-2\Omega\dot{w}+u^2v''-2u\Omega w'-\Omega^2v)+\lambda(x)u(\dot{v}+uv'-\Omega w)+Pv'' + f(x)v''''+2\gamma(x)v'''+\mu(x)v''+\eta(\dot{v}''''+uv'''''')=0\,, \tag{18}$$

$$g(x)(\ddot{w}+2u\dot{w}'+2\Omega\dot{v}+u^2w''+2u\Omega v'-\Omega^2w)+\lambda(x)u(\dot{w}+uw'+\Omega v)+Pw'' + f(x)w''''+2\gamma(x)w'''+\mu(x)w''+\eta(\dot{w}''''+uw'''''')=0. \tag{19}$$

3. Solution procedure

According to the Laplace transform, one can write:

$$L\left[\eta^{(\varepsilon)}(\tau)\right]=s^{\varepsilon}\eta(s)-s^{\varepsilon-1}\eta(0)\,. \tag{20}$$

Hence, the dimensionless governing equation of motion of the system in the Laplace domain, for zero initial conditions, can be rewritten as:

$$g(x)(s^2v+2suv'-2\Omega sw+u^2v''-2u\Omega w'-\Omega^2v)+\lambda(x)u(sv+uv'-\Omega w) + Pv''+f(x)v''''+2\gamma(x)v'''+\mu(x)v''+\eta(sv''''+uv'''''')=0\,, \tag{21}$$

$$g(x)(s^2w + 2usv' + 2\Omega sv + u^2w'' + 2u\Omega v' - \Omega^2 w) + \lambda(x)u(sw + uw' + \Omega v) + Pw'' + f(x)w'''' + 2\gamma(x)w''' + \mu(x)w'' + \eta(sw'''' + uw''''') = 0. \quad (22)$$

To discretize the dynamical equations of motion of the system and obtain the reduced-order model, the Galerkin discretization scheme is utilized. Therefore, the transverse displacements of the system can be approximated by [43, 55, 56]:

$$v(x,t) = \sum_{j=1}^{N} q_j(t)\phi_j(x)\,, \quad (23)$$

$$w(x,t) = \sum_{k=1}^{N} p_k(t)\phi_k(x)\,, \quad (24)$$

where n is the number of basis functions, and q and p are the dimensionless generalized coordinates in the *y*- and *z*- directions, respectively. Also, ϕ is the dimensionless approximation function for the system displacements along *y*- and *z*- directions and is defined for pinned-pinned boundary conditions as [42, 57, 58]:

$$\phi_r(x) = \sqrt{2}\sin(r\pi x)\,. \quad (25)$$

Substituting Eqs. (23) and (24) into Eqs. (21) and (22) and then applying the Galerkin scheme, the dimensionless generalized form of the discretized equations of the system can be expressed in the form:

$$\mathbf{Z}(s) = \begin{bmatrix} \mathbf{K}_1 & \mathbf{K}_2 \\ -\mathbf{K}_2 & \mathbf{K}_1 \end{bmatrix} + s\begin{bmatrix} \mathbf{G}_1 & \mathbf{G}_2 \\ -\mathbf{G}_2 & \mathbf{G}_1 \end{bmatrix} + s^2\begin{bmatrix} \mathbf{M}_1 & \mathbf{0} \\ \mathbf{0} & \mathbf{M}_1 \end{bmatrix}, \quad (26)$$

where $\mathbf{Z}$ denotes the coefficient matrix, and the elements of matrices $\mathbf{M}_1$, $\mathbf{G}_1$, $\mathbf{G}_2$, $\mathbf{K}_1$, and $\mathbf{K}_2$ can be expressed as:

$$(\mathbf{M}_1)_{sr} = \int_0^1 g(x)\phi_s(x)\phi_r(x)\mathrm{d}x\,, \quad (27)$$

$$(\mathbf{G}_1)_{sr} = u\left(\int_0^1 2g(x)\phi_s(x)\phi_r'(x)\mathrm{d}x + \int_0^1 \lambda(\xi)\phi_s(x)\phi_r(x)\mathrm{d}x\right) + \eta\int_0^1 \phi_s(x)\phi_r''''(x)\mathrm{d}x\,, \quad (28)$$

$$(\mathbf{G}_2)_{sr} = -2u\int_0^1 2g(x)\phi_s(x)\phi_r(x)\mathrm{d}x\,, \quad (29)$$

$$(\mathbf{K}_1)_{sr} = u^2 \int_0^1 g(x)\phi_s(x)\phi_r''(x)\mathrm{d}x - \Omega^2 \int_0^1 g(x)\phi_s(x)\phi_r(x)\mathrm{d}x + u^2 \int_0^1 \lambda(x)\phi_s(x)\phi_r'(x)\mathrm{d}x$$
$$+ P\int_0^1 \phi_s(x)\phi_r''(x)\mathrm{d}x + \int_0^1 f(x)\phi_s(x)\phi_r''''(x)\mathrm{d}x + 2\int_0^1 \gamma(x)\phi_s(x)\phi_r'''(x)\mathrm{d}x \quad (30)$$
$$+ \int_0^1 \mu(x)\phi_s(x)\phi_r''(x)\mathrm{d}x + \eta u \int_0^1 \phi_s(x)\phi_r'''''(x)\mathrm{d}x\,,$$

$$(\mathbf{K}_2)_{sr} = -2u\Omega \int_0^1 g(x)\phi_s(x)\phi_r'(x)\mathrm{d}x - u\Omega \int_0^1 \lambda(x)\phi_s(x)\phi_r(x)\mathrm{d}x\,. \quad (31)$$

4. Stability analysis

For the existence of non-trivial solutions, the determinant of the coefficient matrix must be equal to zero. Thus

$$\det[\mathbf{Z}(s)] = \mathbf{0}\,. \quad (32)$$

The complex-valued roots (λ) of Eq. (32) are the eigenvalues of the system and can be calculated in terms of axial load, viscosity coefficient, axial and spin velocities, density and elastic modulus gradient parameters. The imaginary parts of the eigenvalues (ω=Im(λ)) are the damped natural frequencies of the system. The real parts of the eigenvalues (δ=Re(λ)) are related to the damping of the system. It should be mentioned that the system experiences divergence instability when Im(λ)=0. Also, flutter instability occurs in the system when Im(λ)≠0 and Re(λ)>0 [43, 50, 59].

5. Results and discussion

In this section, a comparison study is performed to ensure the accuracy of the presented procedure. Then, the influence of axial load, density and elastic modulus gradations along the beam length on the stability boundaries is clarified. Finally, the effect of material distribution types, viscosity coefficient, axial load, and simultaneous variation of the material properties on the dynamical behaviour of the system are discussed.

5.1. Model validation

Firstly, the natural frequencies of the system are obtained by ignoring the axial material gradation, viscoelastic effect, and external axial load, and are compared with existing results in the literature. The real and imaginary parts of the first four natural frequencies of the homogeneous beam are given in Figures 2 (a-b) when Ω=5. The results of the present study are

in good agreement with those reported by Yang et al. [43]. As shown in Figure 2, compared with axially moving beams and spinning beams, the beams with both axial and spinning motions experience the following stability evolution: stable – first mode divergence – stable – mode-coalescence flutter – stable – first mode divergence – stable – mode-coalescence flutter. Hence, in contrast to mono-gyroscopic systems, bi-gyroscopic systems may experience two different divergence velocities (u_d^1, u_d^2) and two different flutter velocities (u_f^1, u_f^2) as the axial velocity increases.

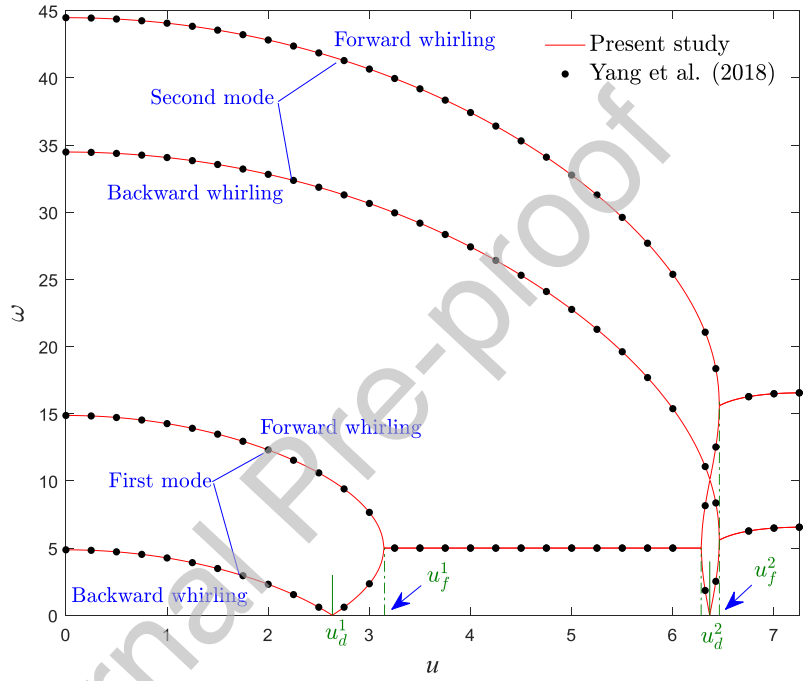

(a)

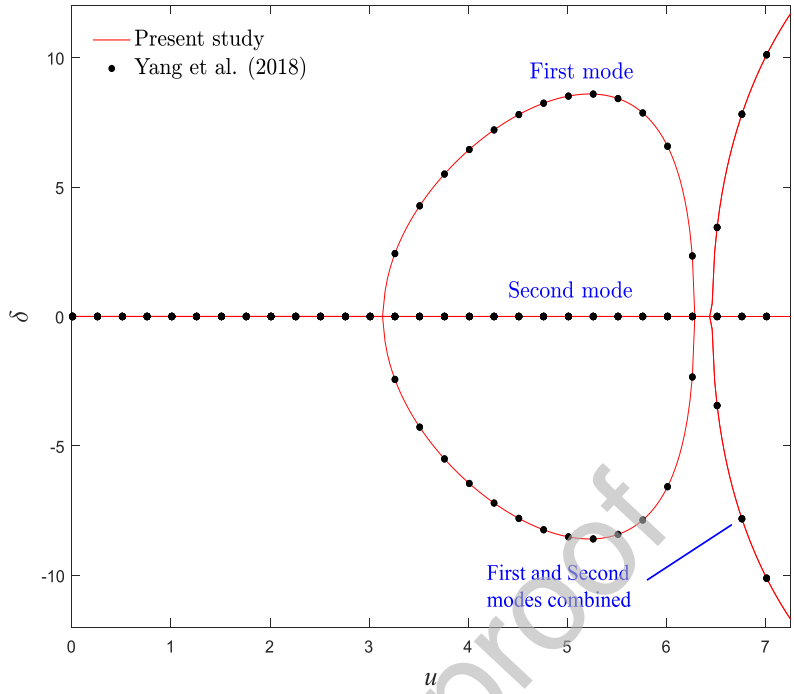

(b)

Fig. 2 (a) Imaginary and (b) real parts of the first four dimensionless eigenvalues of the homogeneous system when ζ=0, P=0, Ω=5, u=2

5.2. Effect of the elastic modulus gradient parameter

In this subsection, it is assumed that the elastic modulus of the system varies linearly along the axial direction. Figures 3 (a-d) show the natural frequencies of the system against the axial velocity for various spin velocities and P=0. As shown in Figure 3a, in the absence of the spin velocity (Ω=0), the fundamental frequency of the system has one branch. Thus, the transverse frequencies of the system coincide. In this case, by increasing the axial velocity, the fundamental frequency of the system decreases monotonically until it vanishes at the critical divergence axial velocity (u_d). As shown in this figure, by increasing the elastic modulus gradient parameter, both the fundamental frequency and the critical divergence axial velocity of the system increase. This trend can be justified by the fact that the elastic modulus gradient parameter only contributes to the stiffness matrix of the system; hence, increasing α_E induces the stiffness-hardening effect in the system and leads to a stiffer system. In other words, by increasing α_E, the divergence strength of the system increases, and the divergence phenomenon occurs at higher axial velocities.

Figures 3(b-d) show that the Coriolis gyroscopic effect causes a bifurcation of the natural frequency when the system has combined axial and spinning motions. As a result, the natural frequency of the system is divided into two separate branches, namely backward whirling (lower branch) and forward whirling (upper branch). In this case, the forward and backward whirling motions occur alternatively for the first two modes, and a traveling wave with spatial configuration can occur. The effect of the axial velocity variation on the natural frequency curves of the system is dramatically dependent on the spin velocity of the system. Figure 3(b) shows that, for small spin velocities (e.g., Ω=5), firstly, by increasing the axial velocity, the backward and forward frequencies of the system decrease gradually reaching to a specific axial velocity (u_d), in which the backward frequency becomes zero and the system experiences the buckling phenomenon. As the axial velocity increases, the system regains its stability immediately. In this condition, as the axial velocity increases further, the backward frequency has an increasing trend, while the forward frequency has a decreasing trend. This trend continues until the lower and upper branches of the natural frequency coincide and merge into a single branch. In this condition, a two-direction coupling flutter happens in the natural frequency diagram. As a result, the system undergoes the flutter phenomenon, and a coupled-mode flutter occurs between the general coordinates in the two transverse directions. In this case, the system displacements become unstable with an oscillatory response. According to Figure 3(b), by increasing α_E, both the critical divergence and the flutter axial velocities increase. Also, for axial velocities lower than the critical divergence axial velocity ($u<u_d$), the axial material gradation has the same influence on the lower and upper branches of the system frequency, so that by increasing α_E, the forward and backward frequencies of the system increase. While for $u>u_d$, this effect is reversed for the lower branch of the natural frequency.

At moderate values of spin velocity, the critical divergence axial velocity of the homogeneous system tends to zero. For example, as demonstrated in Figure 3(c), the critical divergence axial velocity of the homogeneous system becomes zero when Ω=9.87. Consequently, for $\alpha_E>1$, since the divergence phenomenon occurs in the system, the dynamical behaviour of the system and the effect of the axial elastic modulus gradient are similar to that of Figure 3(b). While, for $\alpha_E<1$, the system only experiences the flutter instability, and the divergence instability does not happen. In this case, by increasing the axial velocity, the lower and upper branches increase and decrease,

respectively. For high spin velocities (e.g., Ω=12), since the divergence does not happen in the system, the backward and forward frequencies of the system decrease and increase, respectively, as α_E increases (see Figure 3(d)).

Based on Figures 3 (a-d), by increasing the spin velocity of the system, the natural frequency branches of the system shift to higher frequencies. Therefore, the divergence axial velocity of the system (the intersection between the lower frequency branch and the *x*-axis) decreases by increasing the spin velocity. However, at high spin velocities, the divergence phenomenon does not happen in the system. It should be noted that the spin velocity variation does not affect the critical flutter axial velocity of the system, whereas both the critical divergence and flutter axial velocities can be affected simultaneously by increasing α_E.

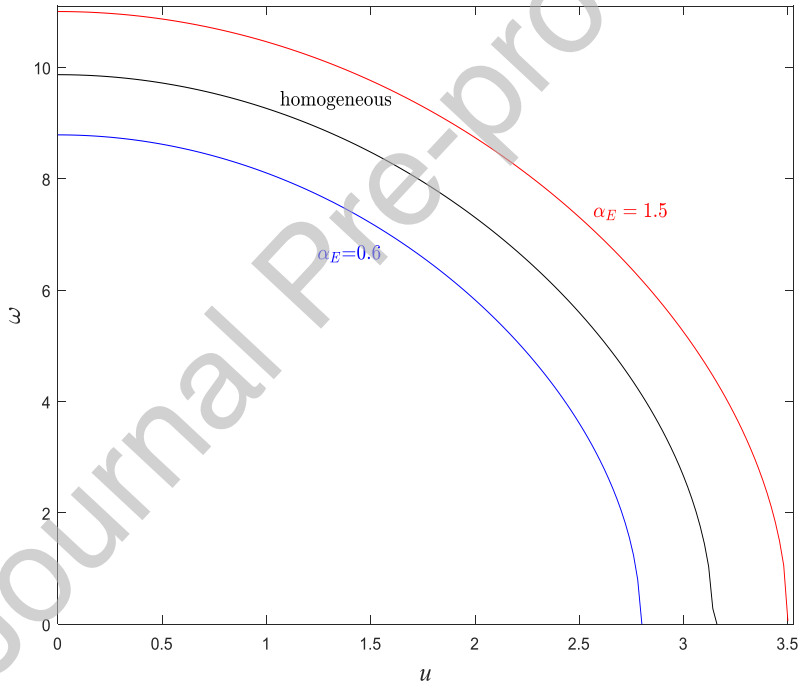

(a)

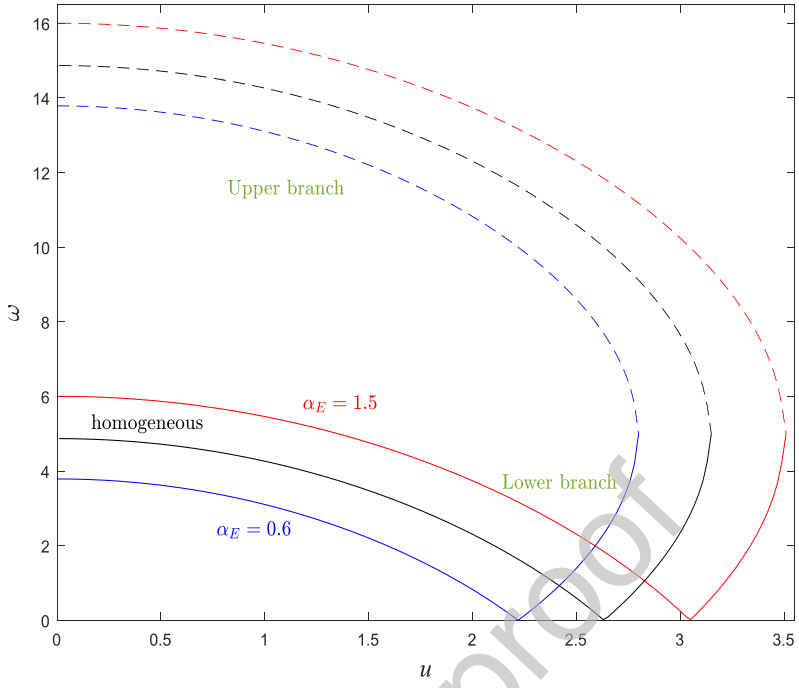

(b)

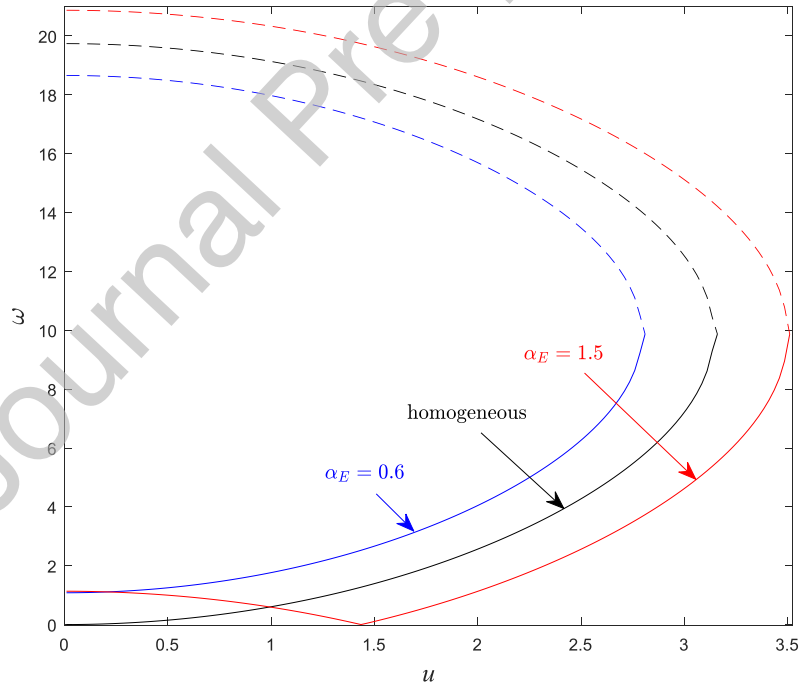

(c)

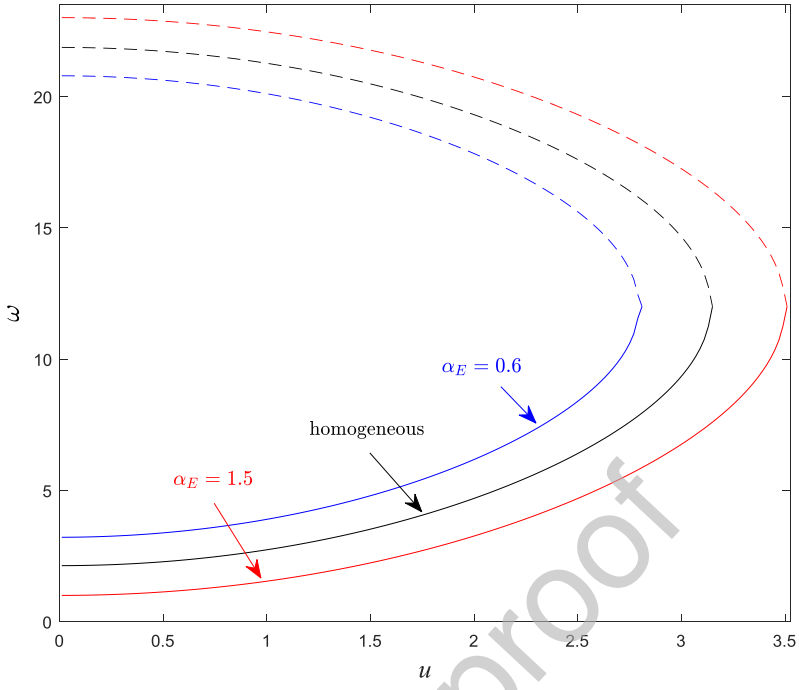

(d)

Fig. 3 Dimensionless natural frequencies of the system versus axial moving velocity when ζ=0, P=0, α_p=1 (a) Ω=0 (b) Ω=5 (c) Ω=9.87 (d) Ω=12

Figure 4 shows the stability map of the system in the u-P plane when Ω=5 and the critical divergence axial velocities and flutter boundaries are given. The system is stable for velocities lower than the first critical divergence axial velocity ($u<u_d^1$). Moreover, the system experiences the flutter instability for velocities higher than the second critical flutter axial velocity ($u<u_f^2$). As the axial compressive load increases, the effective stiffness of the system decreases. As a result, the system stability regions shrink, and the likelihood of divergence and flutter instability increases. In other words, increasing the axial compressive load results in shifting the divergence and the flutter instability borders to lower axial velocities. Additionally, as can be observed in Figure 4, the elastic modulus gradient parameter plays a crucial role in the determination of the stability borders. Compared to homogeneous systems, by increasing α_E, the critical axial velocities of the system tend to move to higher velocities, and the system stability regions expand. It should be emphasized that the effect of the axial material grading on the first critical divergence and flutter axial velocities of the system is more significant.

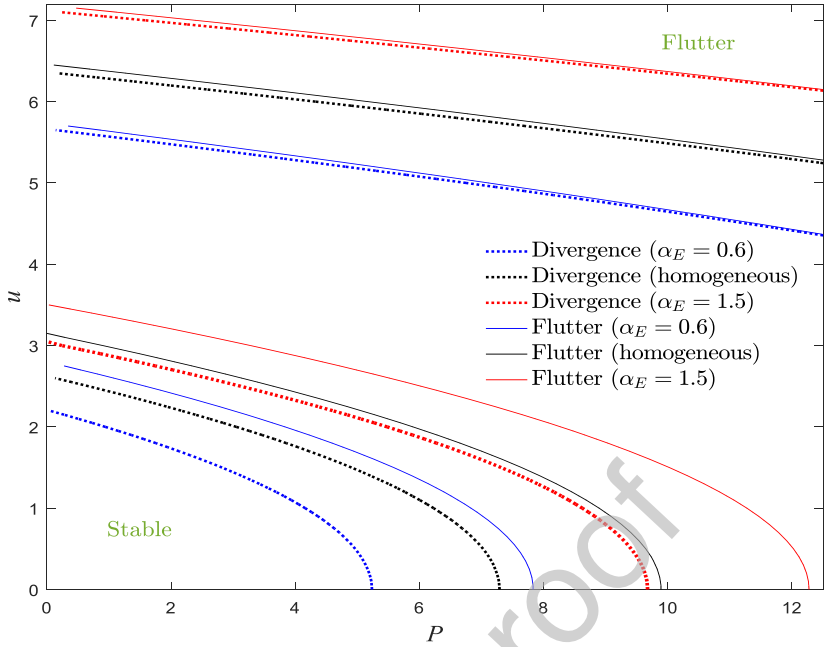

Fig. 4 Dimensionless critical axial velocities of the system versus the axial load when ζ=0, Ω=5, α_ρ=1

Figures 5 (a-b) show the natural frequencies of the AFG beam against the spin velocity for two axial velocities when P=0. Based on Figure 5(a), when the homogeneous system has only spinning motion (i.e., u=0), by increasing the spin velocity, the first forward frequency increases, while the first backward frequency decreases. This trend continues until the first backward frequency becomes zero at a specific spin velocity, and the divergence phenomenon occurs in the system. The corresponding spin velocity is called the divergence spin velocity (Ω_d). Afterward, by further increasing the spin velocity, both the first backward and forward frequencies of the system increase, and the first lower and upper frequency branches become parallel. Since the lower and the upper branches of the natural frequency do not coincide, one can state that the flutter spin velocity of the system is theoretically infinite. As shown in this figure, by decreasing α_E, the divergence spin velocity of the system decreases. Also, for $\Omega<\Omega_d$, by decreasing α_E, both of the first backward and forward frequencies of the system decrease, while for $\Omega>\Omega_d$, the first backward frequency increases with decreasing α_E. This trend occurs similarly for the higher vibrational modes and, for the higher modes, the system experiences the divergence phenomenon at higher spin velocities.

According to Figure 5(b), when the axial velocity increases (e.g., u=3), the first forward frequency of the system decreases in the homogeneous system. In this case, the first backward frequency of the system decreases for $\Omega<\Omega_d$, while increases for $\Omega>\Omega_d$. In other words, at the same spin velocity, by increasing the axial velocity, the first forward frequency of the system decreases. In this condition, the backward frequency of the system for spin velocities lower and higher than the divergence spin velocity, decreases and increases, respectively. Also, by increasing the axial velocity, the divergence spin velocity of the system decreases. Meanwhile, after the divergence phenomenon, by increasing the axial velocity, the natural frequency branches of the system remain parallel. By decreasing α_E, the divergence spin velocity and the forward frequency of the system decreases. Also, by decreasing α_E, for $\Omega<\Omega_d$ and $\Omega>\Omega_d$, the system backward frequency decreases and increases, respectively. Based on Figures 5(a-b), by varying α_E, the natural frequency branches of the system are displaced in parallel. For higher vibrational modes, increasing the axial velocity, decreases the forward frequency. While by increasing u, the backward frequency decreases/increases in the pre/post-buckling condition. Additionally, as can be shown in Figure 5(b), at high axial velocities, by decreasing α_E (e.g., α_E=0.6), the instability divergence phenomenon is not observed in the dynamical behaviour of the system. In this case, the first backward and forward branches coincide, and the system loses its stability via the flutter instability for all spin velocities. Based on Figures 3 and 5, it can be concluded that compared with the homogeneous case, by varying α_E in the AFG systems, the stability evolution of the system can be changed.

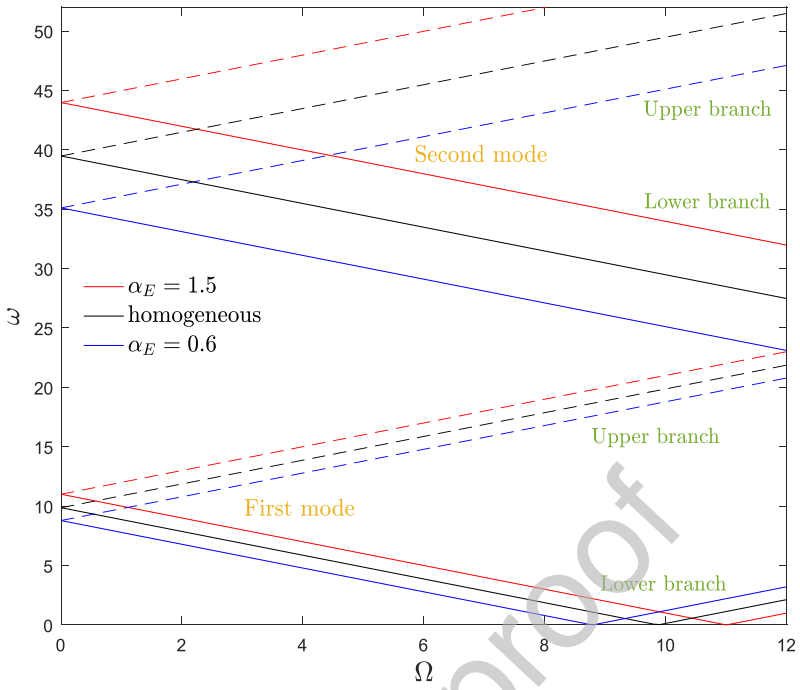

(a)

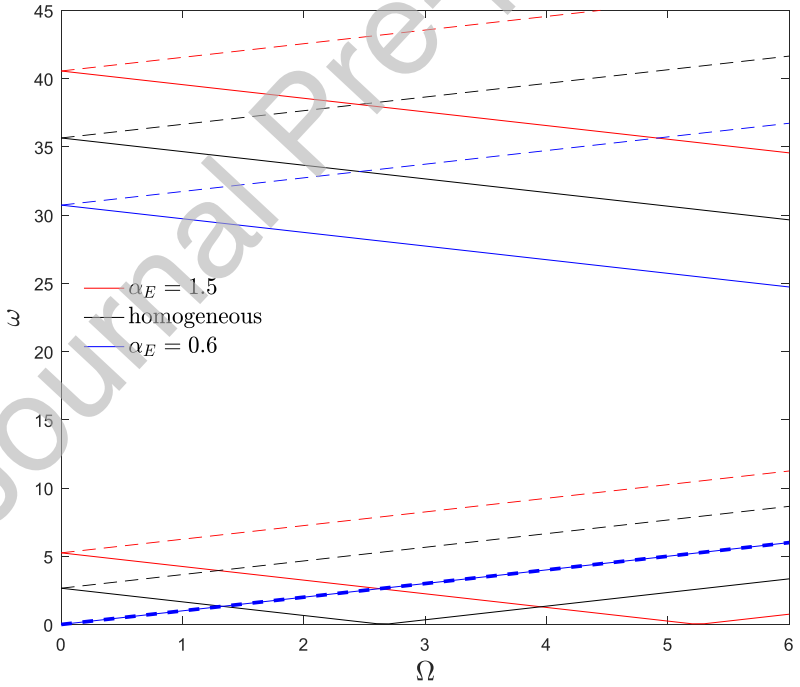

(b)

Fig. 5 Dimensionless natural frequencies of the system versus spin velocity when P=0, ζ=0, α_ρ=1 (a) u=0 (b) u=3

In Figures 6 (a-b), the stability map of the system in the Ω-*P* plane is presented for the first and second vibrational modes, respectively, when u=1. Also, the divergence border and the flutter boundary of the system are given in these figures. In Figure 6 (a), for the homogeneous system, as *P* increases for low spin velocities (i.e., Ω<9.1), the system is initially stable. At a specific axial compressive load, the system experiences the divergence instability. Physically, the beam buckles in both transverse directions through the divergence phenomenon. Then, the system becomes stable again. In other words, for relatively low spin velocities, the initial instability for a conservative system is always of the divergence type. As is evident from this figure, the two stable regions are separated from each other by divergence instability border. So, the divergence phenomenon only occurs on this border, and the divergence instability region does not exist in the stability map. By further increasing the axial compressive load (i.e., *P*>8.9), the system loses its stability via the flutter instability, and the system never regains its stability. In other words, to the right of the vertical lines, the system undergoes the flutter instability. Also, for high spin velocities (e.g., Ω>9.1), the system does not exhibit the divergence type of instability. In this condition, by increasing the axial compressive load, first, the system is stable, and then the flutter instability occurs. Hence, one can state that for low spin velocities (i.e., Ω<9.1), the stability evolution of the homogeneous system is "stable – divergence – flutter". While, for high spin velocities (i.e., Ω>9.1), the stability evolution changes to "stable – flutter". Based on Figure 6, by increasing α_E, the divergence border shifts to higher values of *P* and Ω. Also, since increasing α_E induces the stiffness-hardening effect in the system, the flutter boundaries move to higher axial loads. Additionally, according to Figures 3-6, increasing the spin and axial velocities lead to a decrease in the divergence axial velocity and divergence spin velocity, respectively. According to Figure 6(b), a similar trend occurs for the second vibrational mode, with the difference that the divergence border and flutter threshold of the system occurs at higher spin and axial velocities. It should be mentioned that when the system undergoes flutter for each vibrational mode, the system becomes unstable.

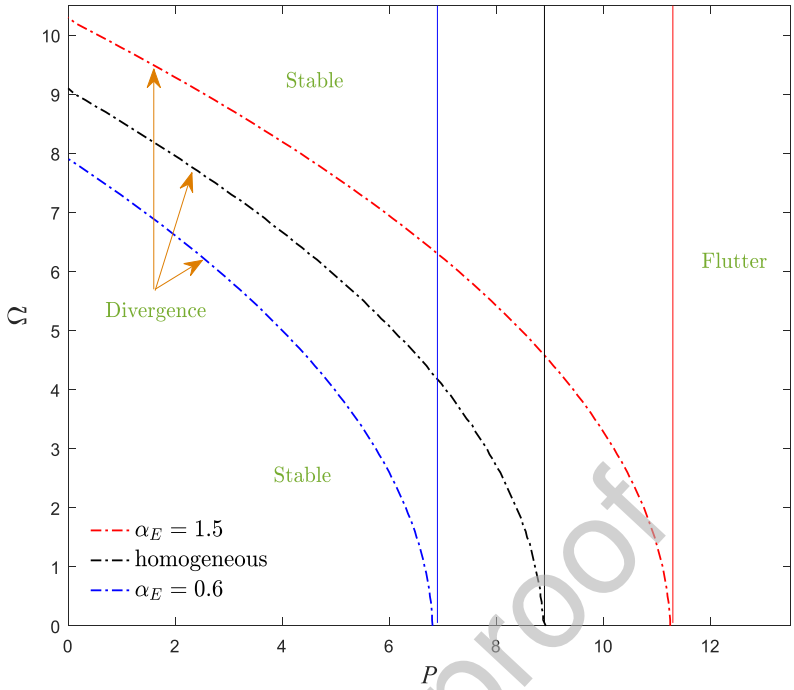

(a)

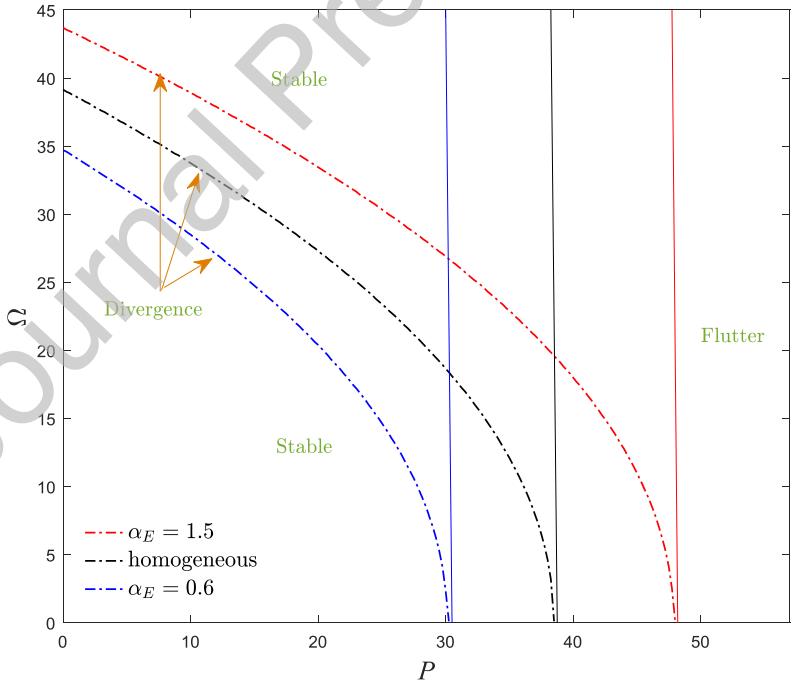

(b)

Fig. 6 Stability map of the system in the Ω-*P* plane for (a) first and (b) second vibrational modes when ζ=0, u=1, α_ρ=1

To better investigate the dynamical behaviour of the system, the divergence spin velocity of the system is plotted against the elastic modulus gradient parameter in Figure 7 for various axial velocities. As observed, by increasing α_E, the divergence spin velocity curves have an increasing trend for all axial velocities. By increasing the axial velocity, the divergence spin velocity of the system decreases. Moreover, at high axial velocities, the divergence spin velocity of the system vanishes for small values of the α_E. In this case, even in the absence of the rotational movement, the axial moving beam is in the flutter instability zone. In this condition, by increasing the axial velocity, the flutter instability boundary extends.

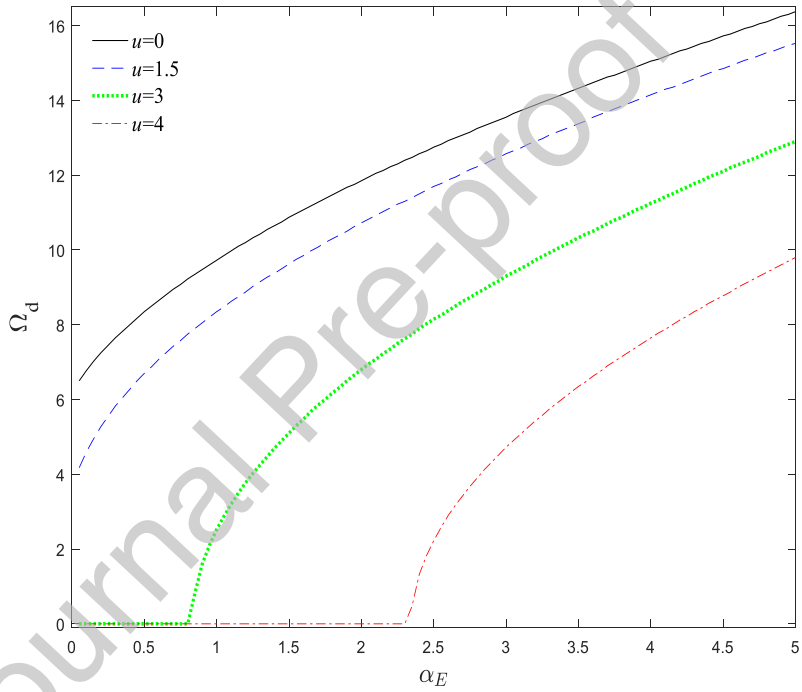

Fig. 7 Dimensionless critical divergence spin velocity of the system versus elastic modulus gradient parameter when ζ=0, P=0, α_ρ=1

5.3. Effect of the density gradient parameter

In this subsection, it is supposed that the system density is graded linearly in the longitudinal direction of the beam. To study the influence of the axial density variation on the vibrational behaviour of the system, for various density gradient parameters, the natural frequency of the system is plotted against the axial velocity in Figure 8 in the absence of the axial compressive load and for Ω=9.5. As can be seen, by increasing α_ρ, the forward frequency of the system

decreases for all axial velocities. Also, for axial velocities lower than the divergence axial velocity ($u<u_d$), by increasing the density gradient parameter, the backward frequency decreases, whereas this pattern is reversed for $u>u_d$. Additionally, the divergence and the flutter axial velocities of the system decrease with increasing α_ρ.

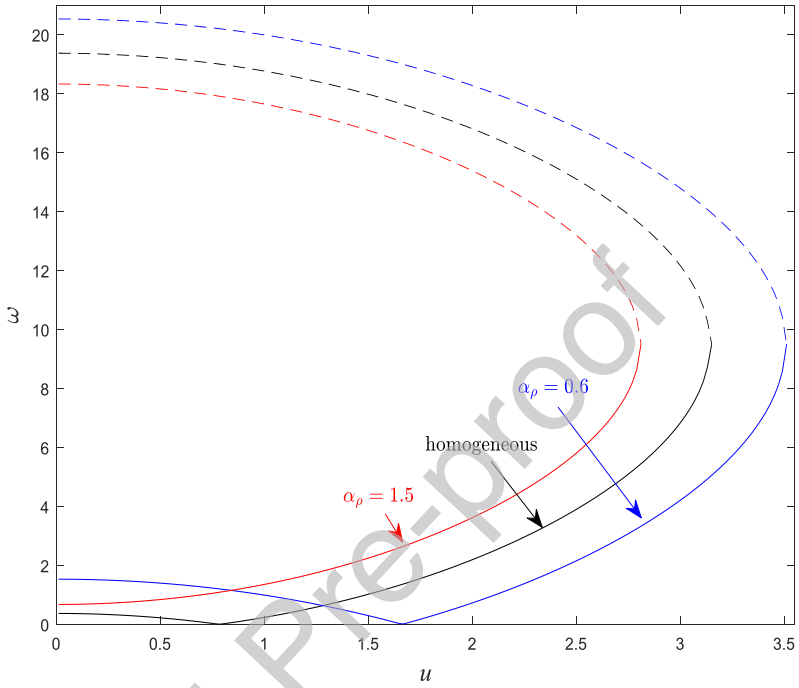

Fig. 8 Dimensionless natural frequencies of the system versus axial velocity when ζ=0, P=0, α_E=1, Ω=9.5

The variations of natural frequencies of the system against the spin velocity are shown in Figure 9 for u=2.5 and various density gradient parameters. Clearly, with the variation of the system density along the beam direction, the natural frequency curves remain parallel. Based on this figure, by increasing α_ρ, the forward frequencies of the system decrease for all values of Ω. Furthermore, by increasing α_ρ, the backward frequencies of the system decrease for the pre-buckling regime, while this trend is reversed for the post-buckling regime. Consequently, it can be stated that the density gradient parameters and the elastic modulus have opposite effects on the vibrational behaviour of the system.

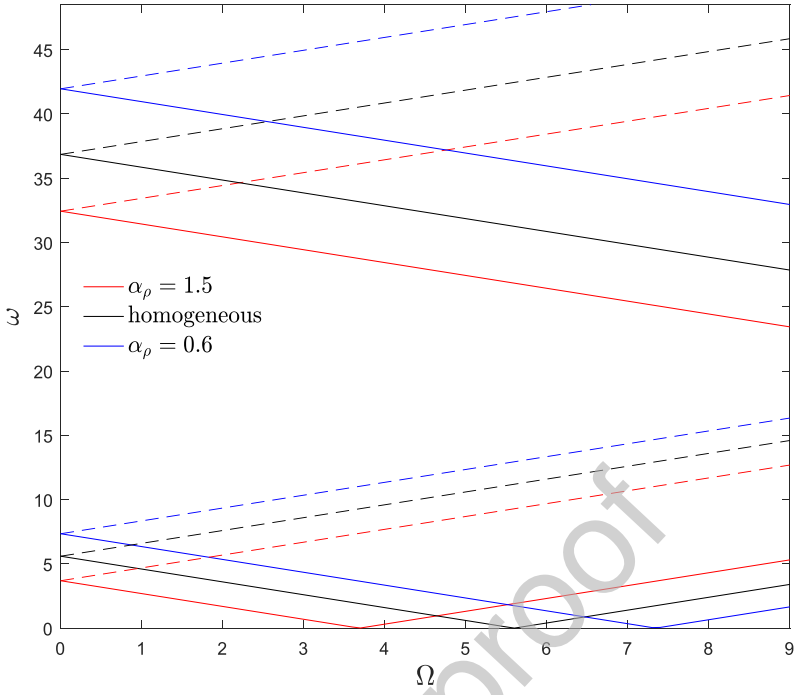

Fig. 9 Dimensionless natural frequencies of the system versus the spin velocity when ζ=0, P=0, u=2.5, α_E=1

To understand the stability of the system in the case of axial density gradation, the divergence spin velocity against the density gradient parameter is displayed in Figure 10 for P=0 and various axial velocities. As expected, by increasing the axial velocity, the divergence spin velocity of the system decreases. This indicates that the reduction of the axial velocity expands the stability region, especially for large values of α_ρ. In other words, the spinning beams without axial motion are more stable in comparison to the spinning and moving beams. Also, it can be seen that for large values of α_ρ, the divergence velocity of the system becomes zero by increasing the axial velocity. In this case, the divergence instability does not occur in the system, and the flutter instability happens for all spin velocities. Another important point in this figure is that in contrast to the Ω_d-α_E curves, the Ω_d-α_ρ curves are overall descending with ascending the density gradient parameter. Therefore, it can be expressed that the density gradient parameter has a decreasing effect on the stability of the system.

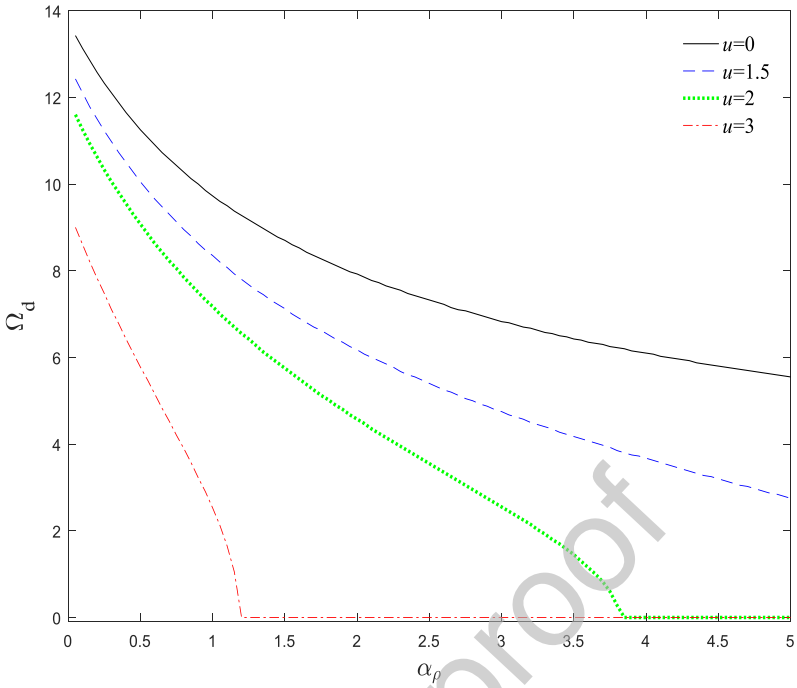

Fig. 10 Dimensionless critical divergence spin velocity of the system versus the density gradient parameter when ζ=0, P=0, α_E=1

To better evaluate the influence of the axial density gradation on the dynamics of the system, the first divergence instability border of the system is presented in Figure 11 for different values of α_ρ and compared with the homogeneous case when P=0. Compared to the homogeneous system, by increasing α_ρ, the divergence phenomenon occurs at lower spin and axial velocities, and vice versa. According to Figures 8-11, the density gradient parameter has a mass-addition effect on the dynamical behaviour of the system; hence, one can conclude that ascending α_ρ has a destabilizing effect on the system. Also, based on Figures 3-11, it can be stated that the increment of elastic modulus gradient, as well as the decrement of the density gradient, are practical approaches to improve the stability behaviour of bi-gyroscopic systems and delay the initiation of the static and dynamic instabilities in the system.

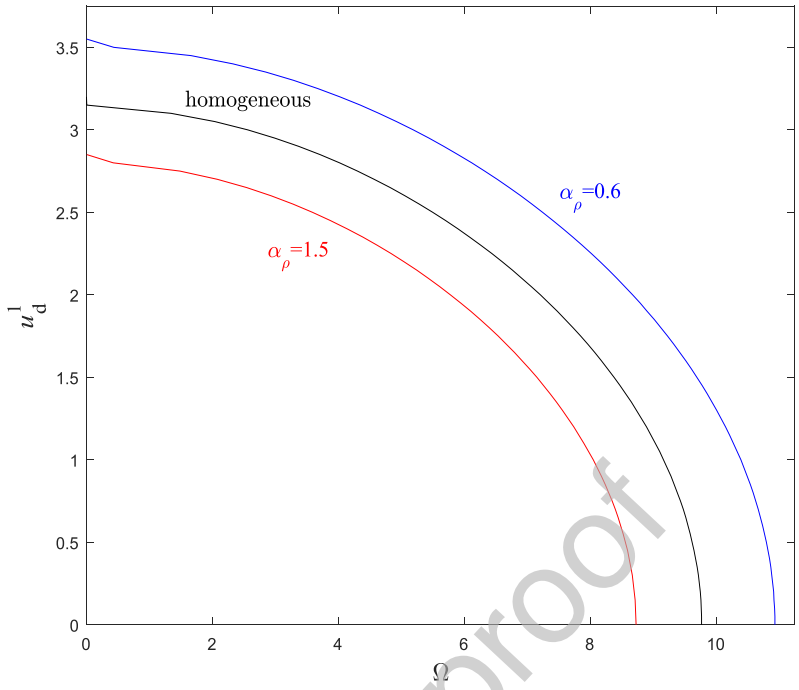

Fig. 11 Effect of density gradient parameter on the first divergence instability border of the system when ζ=0, P=0, α_E=1

5.4. Effect of distribution profile of material characteristics

In this subsection, it is assumed that either the density or the elastic modulus is graded either linearly or exponentially in the axial direction of the system. Figure 12 shows the backward and forward frequencies with linear and exponential distributions of the material properties against the density and elastic modulus gradient parameters for u=1 and Ω=4. By increasing α_E and α_ρ, the natural frequency of the system increases and decreases, respectively. It should be noted that when α_E=1 and α_ρ=1, the considered system degenerates to the homogeneous case and, consequently, the natural frequencies of this system for the linear and exponential distributions of the material properties are equal. Another important feature in this figure is that compared with the exponential elastic modulus distribution, the natural frequencies of the linear elastic modulus distribution are higher, whereas, the natural frequencies for the exponential density distribution are higher than that for the linear density distribution.

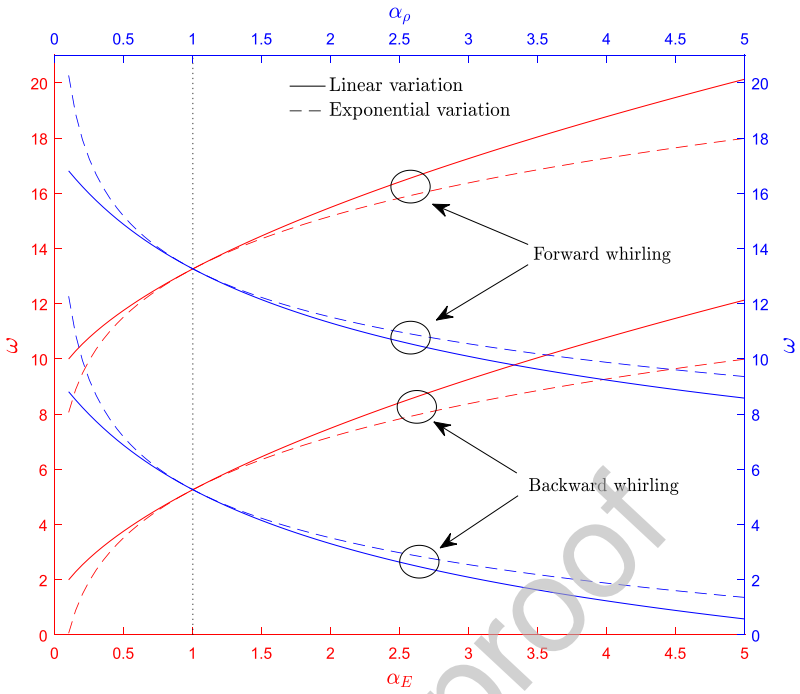

Fig. 12 Dimensionless natural frequencies of the system versus the density and elastic modulus gradient parameters when ζ=0, P=0, u=1, Ω=4

In Figure 13, the effect of the various distributions of the material properties on the first divergence instability border of the system is shown for Ω=2 and P=0. As expected, for the exponential and linear distributions, the divergence borders of the system coincide when α_E=1 and $\alpha\rho$=1. Based on this figure, increasing α_E and decreasing α_ρ expand the stability region of the system. As a result, the system is more stable when α_E>1 and $\alpha\rho$<1. Clearly, in the cases of axial variations of density and elastic modulus, the system is more stable with the exponential and linear distribution profiles, respectively. In other words, for the density variation, the exponential distribution results in a wider stable region, while for the elastic modulus variation, the linear distribution leads to a more stable system.

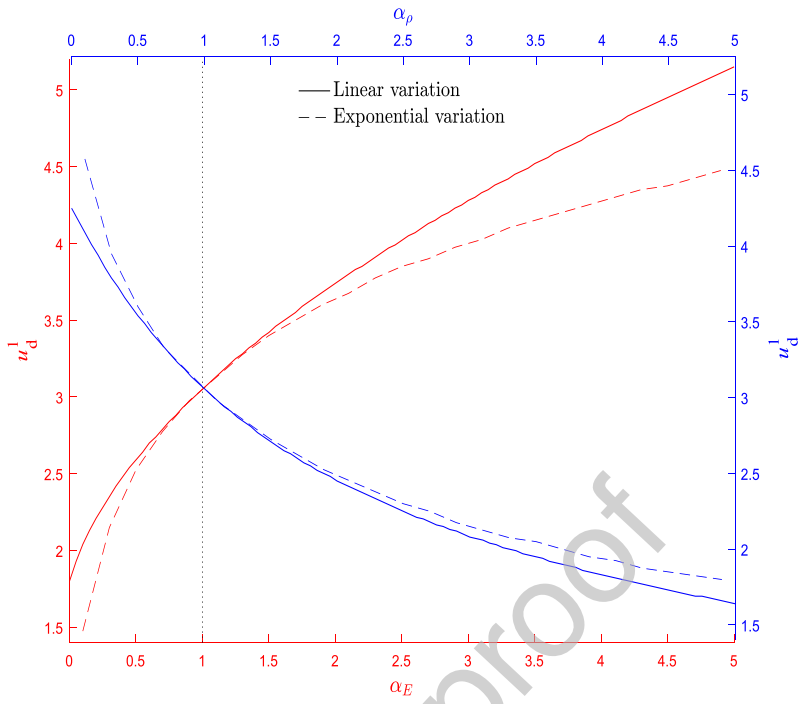

Fig. 13 First dimensionless critical divergence axial velocity of the system versus the density and elastic modulus gradient parameters when ζ=0, P=0, Ω=2

5.5. Effect of simultaneous variation of material properties

In this subsection, it is assumed that the density and elastic modulus gradients are equal (α_ρ=α_{E}=α) and varied simultaneously in the longitudinal direction based on the linear distribution. In Figure 14, the first critical divergence axial velocity of the system against the gradient parameter (α) is given for various axial loads. Clearly, the obtained divergence instability borders using the numerical solution are in good agreement with those acquired by the analytical approach presented in the Appendix. As expected, by decreasing the axial compressive load or increasing the tensile load, the stability region of the system enlarges. In the case of an axial compressive load, increasing the gradient parameter has a stabilizing effect on the system, whereas, in the case of an axial tensile load, increasing the gradient parameter is destabilizing. Therefore, one can conclude that the destabilizing effect of the axial load can be considerably mitigated by the simultaneous determination of the density and the elastic modulus gradients in the axial direction. Also, a rapid change can be observed in the critical divergence axial velocity of the system at small values of the gradient parameter. However, for relatively large α values,

the critical divergence axial velocity loses its sensitivity to the gradient parameter, and for different axial loads, the stability borders of the system are parallel.

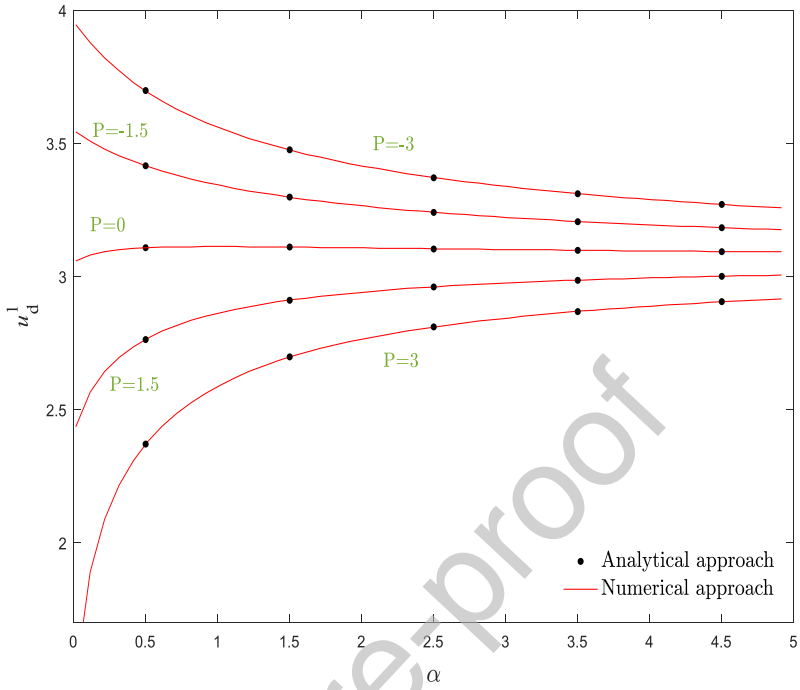

Fig. 14 First dimensionless critical divergence axial velocity of the system versus gradient parameter when ζ=0, Ω=1

5.6. Effect of viscosity

Finally, to investigate the influence of viscoelastic materials on the dynamics of the system, the imaginary and real parts of the first four eigenvalues of the system against the axial velocity are shown in Figures 15(a-b), respectively, for different viscosity coefficients when Ω=1, u=2. Clearly, the critical divergence velocity of the system does not change with the viscoelastic effect of material. This feature can be proved by the presented analytical approach in the Appendix. Since the viscoelastic system is non-conservative, the natural frequencies of the system become complex prior to the occurrence of the divergence phenomenon, especially the natural frequencies of higher modes. Based on Figure 15(b), the imaginary parts of the natural frequency curves lose their symmetry to the x-axis. As shown, the viscoelastic system experiences the stability evolution as "stable – first mode divergence – stable – first mode flutter – first mode divergence – first mode flutter". In addition, the first two natural frequency branches do not merge into a single branch beyond the critical divergence velocity. As a result, it can be

concluded that compared with the homogeneous system, utilizing viscoelastic material changes substantially the stability evolution of the system. Generally, it can be explained that the qualitative stability of axially moving and spinning beams is dependent on the effect of the viscoelastic materials, while axial gradation of materials plays an important role in determining quantitative values of critical velocity and natural frequencies of the system.

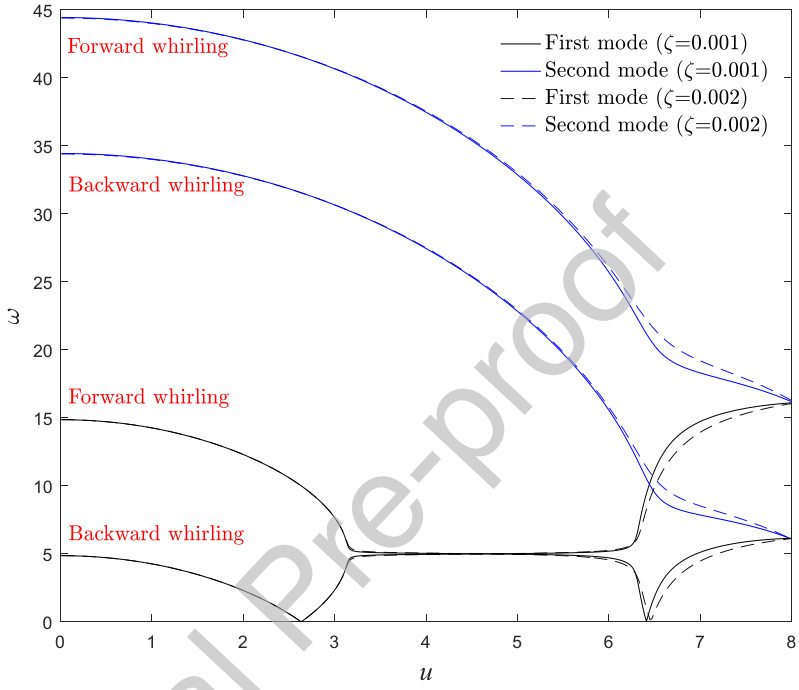

(a)

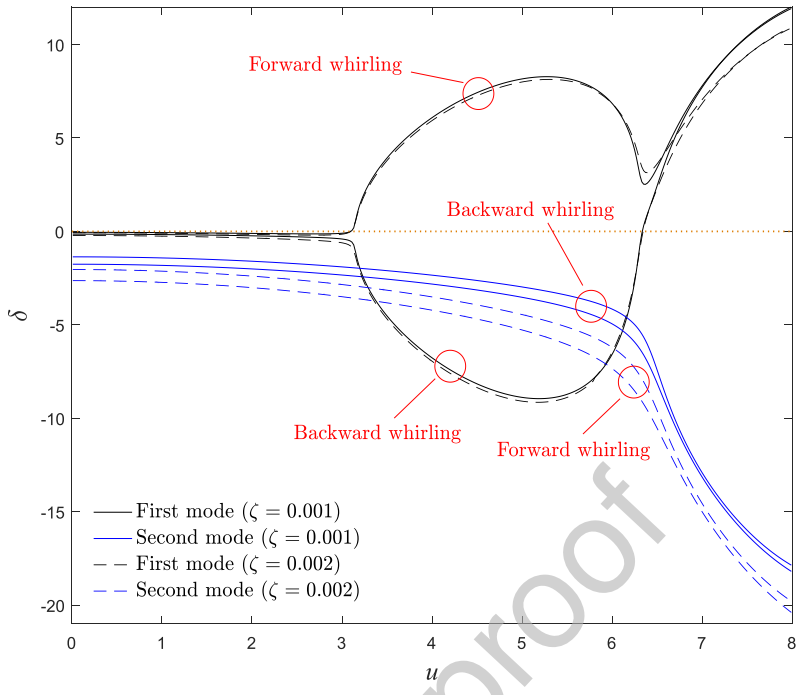

(b)

Fig. 15 (a) Imaginary and (b) real parts of first four eigenvalues of the system when P=0, u=2, Ω=5

6. Conclusion

In this work, a detailed analysis of the dynamical configuration and structural stability of viscoelastic AFG beams with both axial and spinning motions subjected to an external axial load is performed. The Laplace transform, and a Galerkin discretization scheme are employed to solve the model equations. To investigate the divergence and flutter instability conditions, numerical and analytical procedures are applied. The influence of different parameters such as axial grading of the material properties, axial load, viscosity coefficient, axial and spin velocities on the vibrational behaviour of the system is studied. The results revealed that by increasing the elastic modulus and decreasing the density in the longitudinal direction of the system, the forward frequency of the system increases. The effect of axial material gradation on the backward frequency is more complicated. If the system is prone to experience divergence instability, the backward frequency increases/decreases at lower/higher velocities than the critical divergence axial velocity by increasing the elastic modulus gradient parameter and decreasing the density gradient parameter. Otherwise, increasing/decreasing the elastic

modulus/density gradient parameter leads to a reduction in the backward frequency. It is understood that an increase in the density and elastic modulus gradient parameters has destabilizing and stabilizing effects on the system, respectively. In other words, compared with the homogeneous systems, the AFG system is more stable when the density decreases and the elastic modulus increases in the longitudinal direction. In addition, in the case of density/elastic modulus variation, the exponential/linear distribution leads to a more stable system and higher frequencies. It is concluded that the variation of spin velocity does not affect the flutter instability threshold of the system. It is demonstrated that by accurately adjusting the axial gradation of material, the divergence instability in the system can be eliminated, and the flutter instability threshold can be delayed. Additionally, it is shown that by utilizing the viscoelastic material in the system, the stability evolution of the system can be drastically altered. Also, the obtained results indicated that by determining the density and the elastic modulus gradients in the longitudinal direction simultaneously, the destructive effects of the axial compressive load could be considerably alleviated. The modelling and results of the present research could be helpful in the design of viscoelastic inhomogeneous bi-gyroscopic continua.

Appendix

When the system has the critical divergence spin or axial velocity, the lowest natural frequency of the system, (i.e., the backward frequency) becomes zero. This implies that the system loses its stiffness in the primary mode. As a result, to extract analytically the critical divergence velocity related to the first mode, Eq. (26) is reduced to the following equation by considering one mode (r=s=1):

$$\mathbf{Z}_{11} = \begin{bmatrix} k_{11} & k_{12} \\ -k_{12} & k_{11} \end{bmatrix} + \begin{bmatrix} g_{11} & g_{12} \\ -g_{12} & g_{11} \end{bmatrix} + \begin{bmatrix} m_{11} & 0 \\ 0 & m_{11} \end{bmatrix}. \tag{A.1}$$

By considering the linear variation of the material properties, elements can be written:

$$k_{11} = \pi^4(\alpha_E + 1) - \pi^2\left((\alpha_\rho + 1)u^2 + 2P\right) - \Omega^2(\alpha_\rho + 1), \tag{A.2}$$

$$k_{12} = -6u\Omega(\alpha_\rho - 1). \tag{A.3}$$

According to the stability theory of the linear gyroscopic systems [60], when the eigenvalues of the system are zero, the determinant of the stiffness matrix becomes zero. Therefore, the critical divergence spin or axial velocity of the system can be obtained from the following relation:

$$k_{11}k_{22} - k_{12}k_{21} = 0. \quad \text{(A.6)}$$

References:

[1] M. H. Ghayesh and S. Balar, "Non-linear parametric vibration and stability analysis for two dynamic models of axially moving Timoshenko beams," *Applied Mathematical Modelling,* vol. 34, pp. 2850-2859, 2010.

[2] S. Kazemirad, M. H. Ghayesh, and M. Amabili, "Thermo-mechanical nonlinear dynamics of a buckled axially moving beam," *Archive of Applied Mechanics,* vol. 83, pp. 25-42, 2013.

[3] M. H. Ghayesh, "Stability and bifurcations of an axially moving beam with an intermediate spring support," *Nonlinear Dynamics,* vol. 69, pp. 193-210, 2012.

[4] K. Marynowski and T. Kapitaniak, "Dynamics of axially moving continua," *International Journal of Mechanical Sciences,* vol. 81, pp. 26-41, 2014.

[5] L.-Q. Chen, "Analysis and control of transverse vibrations of axially moving strings," *Applied Mechanics Reviews,* vol. 58, pp. 91-116, 2005.

[6] M. H. Ghayesh and M. Amabili, "Nonlinear vibrations and stability of an axially moving Timoshenko beam with an intermediate spring support," *Mechanism and Machine Theory,* vol. 67, pp. 1-16, 2013.

[7] M. H. Ghayesh and M. Amabili, "Nonlinear dynamics of an axially moving Timoshenko beam with an internal resonance," *Nonlinear Dynamics,* vol. 73, pp. 39-52, 2013.

[8] M. H. Ghayesh and M. Amabili, "Post-buckling bifurcations and stability of high-speed axially moving beams," *International Journal of Mechanical Sciences,* vol. 68, pp. 76-91, 2013.

[9] S. Shahedi and M. Mohammadimehr, "Vibration analysis of rotating fully-bonded and delaminated sandwich beam with CNTRC face sheets and AL-foam flexible core in thermal and moisture environments," *Mechanics Based Design of Structures and Machines,* pp. 1-31, 2019.

[10] A. G. Shenas, S. Ziaee, and P. Malekzadeh, "Vibrational behavior of rotating pre-twisted functionally graded microbeams in thermal environment," *Composite Structures,* vol. 157, pp. 222-235, 2016.

[11] M. H. Tsai, W. Y. Lin, Y. C. Zhou, and K. M. Hsiao, "Investigation on steady state deformation and free vibration of a rotating inclined Euler beam," *International journal of mechanical sciences,* vol. 53, pp. 1050-1068, 2011.

[12] M. Shahgholi and S. Khadem, "Internal, combinational and sub-harmonic resonances of a nonlinear asymmetrical rotating shaft," *Nonlinear Dynamics,* vol. 79, pp. 173-184, 2015.

[13] D. Younesian and E. Esmailzadeh, "Non-linear vibration of variable speed rotating viscoelastic beams," *Nonlinear Dynamics,* vol. 60, pp. 193-205, 2010.

[14] S. Faroughi, A. Rahmani, and M. Friswell, "On wave propagation in two-dimensional functionally graded porous rotating nano-beams using a general nonlocal higher-order beam model," *Applied Mathematical Modelling,* vol. 80, pp. 169-190, 2020.

[15] A. Abbasi, S. Khadem, S. Bab, and M. Friswell, "Vibration control of a rotor supported by journal bearings and an asymmetric high-static low-dynamic stiffness suspension," *Nonlinear Dynamics,* vol. 85, pp. 525-545, 2016.

[16] M. H. Ghayesh, "Viscoelastic mechanics of Timoshenko functionally graded imperfect microbeams," *Composite Structures,* vol. 225, p. 110974, 2019.

[17] M. H. Ghayesh, "Mechanics of viscoelastic functionally graded microcantilevers," *European Journal of Mechanics-A/Solids,* vol. 73, pp. 492-499, 2019.

[18] A. Ebrahimi-Mamaghani, S. H. Mirtalebi, and M.-T. Ahmadian, "Magneto-mechanical stability of axially functionally graded supported nanotubes," *Materials Research Express,* vol. 6, p. 1250c5, 2020.

[19] A. Ebrahimi-Mamaghani, H. Sarparast, and M. Rezaei, "On the vibrations of axially graded Rayleigh beams under a moving load," *Applied Mathematical Modelling,* vol. 84, pp. 554-570, 2020.
[20] A. Ebrahimi-Mamaghani, R. Sotudeh-Gharebagh, R. Zarghami, and N. Mostoufi, "Thermo-mechanical stability of axially graded Rayleigh pipes," *Mechanics Based Design of Structures and Machines*, pp. 1-30, 2020.
[21] S. Esfahani, S. E. Khadem, and A. E. Mamaghani, "Nonlinear vibration analysis of an electrostatic functionally graded nano-resonator with surface effects based on nonlocal strain gradient theory," *International Journal of Mechanical Sciences,* vol. 151, pp. 508-522, 2019.
[22] S. H. Mirtalebi, A. Ebrahimi-Mamaghani, and M. T. Ahmadian, "Vibration Control and Manufacturing of Intelligibly Designed Axially Functionally Graded Cantilevered Macro/Micro-tubes," *IFAC-PapersOnLine,* vol. 52, pp. 382-387, 2019.
[23] M. H. Ghayesh, "Nonlinear vibration analysis of axially functionally graded shear-deformable tapered beams," *Applied Mathematical Modelling,* vol. 59, pp. 583-596, 2018.
[24] M. H. Ghayesh, "Dynamics of functionally graded viscoelastic microbeams," *International Journal of Engineering Science,* vol. 124, pp. 115-131, 2018.
[25] M. H. Ghayesh, "Functionally graded microbeams: simultaneous presence of imperfection and viscoelasticity," *International Journal of Mechanical Sciences,* vol. 140, pp. 339-350, 2018.
[26] M. T. Piovan and R. Sampaio, "Vibrations of axially moving flexible beams made of functionally graded materials," *Thin-Walled Structures,* vol. 46, pp. 112-121, 2008.
[27] K. Kiani, "Longitudinal and transverse instabilities of moving nanoscale beam-like structures made of functionally graded materials," *Composite Structures,* vol. 107, pp. 610-619, 2014.
[28] S. Sui, L. Chen, C. Li, and X. Liu, "Transverse vibration of axially moving functionally graded materials based on Timoshenko beam theory," *Mathematical Problems in Engineering,* vol. 2015, 2015.
[29] T. Yan, T. Yang, and L. Chen, "Direct Multiscale Analysis of Stability of an Axially Moving Functionally Graded Beam with Time-Dependent Velocity," *Acta Mechanica Solida Sinica,* pp. 1-14.
[30] M. Asghari and E. Ghafoori, "A three-dimensional elasticity solution for functionally graded rotating disks," *Composite Structures,* vol. 92, pp. 1092-1099, 2010.
[31] L. Li and D. Zhang, "Dynamic analysis of rotating axially FG tapered beams based on a new rigid–flexible coupled dynamic model using the B-spline method," *Composite Structures,* vol. 124, pp. 357-367, 2015.
[32] N. Shafiei, A. Mousavi, and M. Ghadiri, "Vibration behavior of a rotating non-uniform FG microbeam based on the modified couple stress theory and GDQEM," *Composite Structures,* vol. 149, pp. 157-169, 2016.
[33] F. Ebrahimi and M. Mokhtari, "Transverse vibration analysis of rotating porous beam with functionally graded microstructure using the differential transform method," *Journal of the Brazilian Society of Mechanical Sciences and Engineering,* vol. 37, pp. 1435-1444, 2015.
[34] H. Zarrinzadeh, R. Attarnejad, and A. Shahba, "Free vibration of rotating axially functionally graded tapered beams," *Proceedings of the Institution of Mechanical Engineers, Part G: Journal of Aerospace Engineering,* vol. 226, pp. 363-379, 2012.
[35] S.-Y. Oh, L. Librescu, and O. Song, "Vibration and instability of functionally graded circular cylindrical spinning thin-walled beams," *Journal of sound and vibration,* vol. 285, pp. 1071-1091, 2005.
[36] M. Ramesh and N. M. Rao, "Free vibration analysis of pre-twisted rotating FGM beams," *International journal of Mechanics and Materials in Design,* vol. 9, pp. 367-383, 2013.
[37] S.-Y. Oh, L. Librescu, and O. Song, "Vibration of turbomachinery rotating blades made-up of functionally graded materials and operating in a high temperature field," *Acta Mechanica,* vol. 166, pp. 69-87, 2003.

[38] M. Azimi, S. S. Mirjavadi, N. Shafiei, and A. Hamouda, "Thermo-mechanical vibration of rotating axially functionally graded nonlocal Timoshenko beam," *Applied Physics A*, vol. 123, p. 104, 2017.
[39] L. Librescu, S. Y. Oh, and O. Song, "Spinning thin-walled beams made of functionally graded materials: modeling, vibration and instability," *European Journal of Mechanics-A/Solids*, vol. 23, pp. 499-515, 2004.
[40] J. Yuh and T. Young, "Dynamic modeling of an axially moving beam in rotation: simulation and experiment," *Journal of Dynamic Systems, Measurement, and Control*, vol. 113, pp. 34-40, 1991.
[41] H. Lee, "Vibration of a pretwisted spinning and axially moving beam," *Computers & structures*, vol. 52, pp. 595-601, 1994.
[42] K. Zhu and J. Chung, "Vibration and stability analysis of a simply-supported Rayleigh beam with spinning and axial motions," *Applied Mathematical Modelling*, vol. 66, pp. 362-382, 2019.
[43] X.-D. Yang, J.-H. Yang, Y.-J. Qian, W. Zhang, and R. V. Melnik, "Dynamics of a beam with both axial moving and spinning motion: An example of bi-gyroscopic continua," *European Journal of Mechanics-A/Solids*, vol. 69, pp. 231-237, 2018.
[44] M. H. Ghayesh, M. R. Ghazavi, and S. E. Khadem, "Non-linear vibration and stability analysis of an axially moving rotor in sub-critical transporting speed range," *Structural Engineering and Mechanics*, vol. 34, pp. 507-523, 2010.
[45] S. Sahebkar, M. Ghazavi, S. Khadem, and M. Ghayesh, "Nonlinear vibration analysis of an axially moving drillstring system with time dependent axial load and axial velocity in inclined well," *Mechanism and Machine Theory*, vol. 46, pp. 743-760, 2011.
[46] X. Li, Y. Qin, Y. Li, and X. Zhao, "The coupled vibration characteristics of a spinning and axially moving composite thin-walled beam," *Mechanics of Advanced Materials and Structures*, vol. 25, pp. 722-731, 2018.
[47] M. Rezaee and S. Lotfan, "Non-linear nonlocal vibration and stability analysis of axially moving nanoscale beams with time-dependent velocity," *International Journal of Mechanical Sciences*, vol. 96, pp. 36-46, 2015.
[48] M. H. Ghayesh, "Nonlinear forced dynamics of an axially moving viscoelastic beam with an internal resonance," *International Journal of Mechanical Sciences*, vol. 53, pp. 1022-1037, 2011.
[49] R. F. Zinati, M. Rezaee, and S. Lotfan, "Nonlinear Vibration and Stability Analysis of Viscoelastic Rayleigh Beams Axially Moving on a Flexible Intermediate Support," *Iranian Journal of Science and Technology, Transactions of Mechanical Engineering*, pp. 1-15, 2019.
[50] F. Liang, X.-D. Yang, Y.-J. Qian, and W. Zhang, "Transverse free vibration and stability analysis of spinning pipes conveying fluid," *International Journal of Mechanical Sciences*, vol. 137, pp. 195-204, 2018.
[51] M. I. Othman and M. Fekry, "Effect of rotation and gravity on generalized thermo-viscoelastic medium with voids," *Multidiscipline Modeling in Materials and Structures*, 2018.
[52] M. I. Othman, M. Fekry, and M. Marin, "Plane waves in generalized magneto-thermo-viscoelastic medium with voids under the effect of initial stress and laser pulse heating," *Structural Engineering and Mechanics*, vol. 73, pp. 621-629, 2020.
[53] H. Sarparast and A. Ebrahimi-Mamaghani, "Vibrations of laminated deep curved beams under moving loads," *Composite Structures*, vol. 226, p. 111262, 2019.
[54] R. Bahaadini and A. R. Saidi, "On the stability of spinning thin-walled porous beams," *Thin-Walled Structures*, vol. 132, pp. 604-615, 2018.
[55] A. E. Mamaghani, S. Khadem, and S. Bab, "Vibration control of a pipe conveying fluid under external periodic excitation using a nonlinear energy sink," *Nonlinear Dynamics*, vol. 86, pp. 1761-1795, 2016.
[56] R. Hosseini, M. Hamedi, A. Ebrahimi Mamaghani, H. C. Kim, J. Kim, and J. Dayou, "Parameter identification of partially covered piezoelectric cantilever power scavenger based on the coupled distributed parameter solution," *International Journal of Smart and Nano Materials*, vol. 8, pp. 110-124, 2017.

[57] S. Esfahani, S. Esmaeilzade Khadem, and A. Ebrahimi Mamaghani, "Size-dependent nonlinear vibration of an electrostatic nanobeam actuator considering surface effects and inter-molecular interactions," *International Journal of Mechanics and Materials in Design*, vol. 15, pp. 489-505, 2019.
[58] A. E. Mamaghani, S. E. Khadem, S. Bab, and S. M. Pourkiaee, "Irreversible passive energy transfer of an immersed beam subjected to a sinusoidal flow via local nonlinear attachment," *International Journal of Mechanical Sciences*, vol. 138, pp. 427-447, 2018.
[59] A. Ebrahimi-Mamaghani, R. Sotudeh-Gharebagh, R. Zarghami, and N. Mostoufi, "Dynamics of two-phase flow in vertical pipes," *Journal of Fluids and Structures*, vol. 87, pp. 150-173, 2019.
[60] P. Lancaster, "Stability of linear gyroscopic systems: A review," *Linear Algebra and its Applications*, vol. 439, pp. 686-706, 2013.